Available online at www.sciencedirect.com
SCIENCE DIRECT®
Mechanism and Machine Theory 41 (2006) 119–144
Mechanism and Machine Theory
www.elsevier.com/locate/mechmt

Performance atlases and optimum design of planar 5R symmetrical parallel mechanisms

Xin-Jun Liu [a,*], Jinsong Wang [a], G. Pritschow [b]

[a] *Manufacturing Engineering Institute, Department of Precision Instruments, Tsinghua University, Beijing 100084, PR China*
[b] *Institut für Steuerungstechnik (ISW), University of Stuttgart, Seidenstr. 36, D-70174 Stuttgart, Germany*

Received 16 November 2004; received in revised form 7 April 2005; accepted 1 May 2005
Available online 28 June 2005

Abstract

This paper addresses the graphical representation of performances and the optimum design issue of the planar 5R symmetrical parallel mechanism. In this the paper, some performance indices, such as the *global conditioning index* (GCI), *the global velocity index* (GVI), *the global payload index* (GPI), and the *global stiffness (deformation) index* (GSI), will be defined and investigated. The corresponding atlases will be finally represented graphically in the established design space. Based on these atlases, one can synthesize the link lengths of the studied mechanism with respect to specified criteria. Some examples will be given to show how to use the atlases. Especially, an example will be presented to achieve the optimum dimensional mechanism with respect to a desired workspace based on the optimum non-dimensional result obtained from the atlases. For the reason that using the atlases presented in this paper a designer can obtain the optimum result with respect to any object(s), the optimum design method proposed in this paper can be accepted by others.

Keywords: Parallel mechanism; Optimum design; Performance atlas; Velocity; Payload capability; Stiffness

* Corresponding author.
E-mail address: xinjunl@yahoo.com (X.-J. Liu).

0094-114X/$ - see front matter © 2005 Elsevier Ltd. All rights reserved.
doi:10.1016/j.mechmachtheory.2005.05.003

1. Introduction

In the design process of a mechanism, the performance index will be inevitably involved. In numerical analysis, the condition number can estimate the error generated in the solution of a linear system of equations by the error on the data [1]. When applied to the Jacobian matrix, the condition number will give a measure of the control accuracy of a mechanism [2]. It can evaluate the dexterity and isotropy of a mechanism as well [3–6]. Then, the conditioning index, which is the reciprocal of the condition number, is usually used as the prior criterion in the optimum design of a mechanism by most researchers. For some applications, other indices, such as accuracy [7] and stiffness [8] may be considered. In order to evaluate the performance of a mechanism within a workspace, a global conditioning index was defined [9]. Following this definition, the global indices for velocity, payload capability and stiffness will be defined in this paper.

No matter how simple the 5R symmetrical parallel mechanism is, the optimum design is always challenging. Many efforts have been contributed to this issue. For example, Gao et al. [10,11] and Liu [12] developed a solution space trying to solve the optimum design by means of performance atlases. The solution space is a good idea. However, due to unreasonable workspace presentation, the reported performance atlases cannot be applied to the practical design. Cervantes-Sánchez et al. [13] established a space made up of two normalized geometric parameters to show the characteristics of workspace and singularity. Due to its infinity, the space cannot include all *similarity mechanisms*[1] in a finite space. Therefore, the tool is not good enough for the optimum design. Besides this disadvantage, the workspace and singularity plotted in the space are in general forms, from which one cannot identify the performances of the mechanism with specified inverse and forward kinematic modes. They cannot be used in the practical design as well. Other types of synthesis charts have been presented for the design of the 5R mechanism in Refs. [14–16]. They may not yield mechanisms that have some desired benefits such as dexterity, singularity-free workspace, payload capability, velocity and stiffness. Recently, the optimum design issue of the 5R symmetrical parallel mechanism was investigated in Ref. [17,18]. In [17], a hybrid method, implemented in two steps, was proposed to optimize the mechanism with respect to the local and global conditioning indices. In the first step, a set of parameter relationships in closed form that enable the number of involved design parameters to be reduced was established to find an optimal architecture. In their second step, a good-conditioning workspace with a specified conditioning index could be obtained thanks to only one parameter. In [18], an optimum procedure was reported to obtain the optimum results with respect to the ideal/isotropic condition number and bearing forces for force balancing. This method is a traditional one, implemented in the commercial software MATLAB based on an established object function. The two methods, which may be good to achieve an optimal result, were failed to illustrate the relationship between an index and the involved design parameters. The reader cannot know how optimal their results are. If the design criterion number is increased, the procedure will be more complicated. And if the object function is different, a designer should start the optimization from the very beginning. For such reasons, the proposed procedures are difficult to be accepted being as a unified methodology.

[1] In this paper, *similarity mechanisms* are defined as the mechanisms that are similar in size and performances.

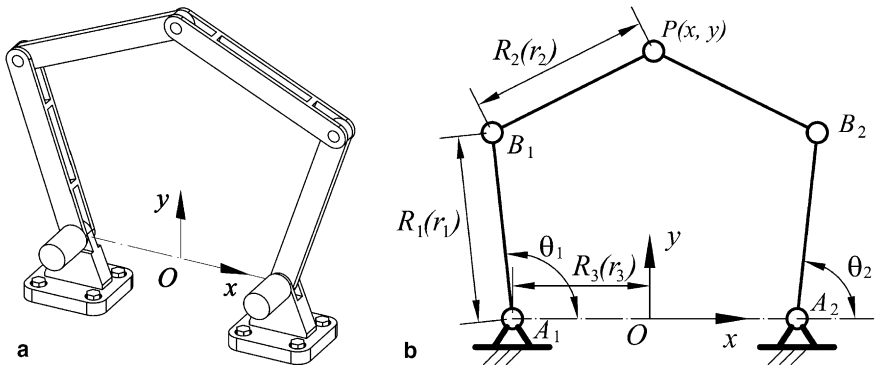

Fig. 1. The planar 5R symmetrical parallel mechanism.

In Ref. [19], a design space for the planar 5R symmetrical parallel mechanism shown in Fig. 1 was established in a finite space. After normalization, a mechanism with any group of link lengths can find its position in this space. Therefore, the space makes it possible to illustrate the relationship between a performance index and link lengths of the mechanism. This is the most important reason why it can be applied in the optimum design of the mechanism. In this paper, performance atlases for the conditioning index, velocity, payload capability and stiffness will be represented in the design space. The atlases can be directly used in the design procedure. Some examples showing how to use these atlases will be presented. Especially, an example will be given to achieve the optimum dimensional result with respect to a desired workspace based on the optimum non-dimensional result obtained from the atlases. Because, using the atlases presented in this paper, a designer can obtain the optimum result with respect to any object(s). The optimum design method proposed in this paper shall be said to be acceptable in practice.

2. Performance indices and atlases

The workspace performance of the 5R parallel mechanism has been studied in Ref. [19], where the *maximal inscribed workspace* (MIW) is defined as the circular region bounded by the *maximal inscribed circle* (MIC).[2] And the atlases of the MIW area and distribution of the workspace shape have been presented. In the design process, workspace is usually not the only desired performance. Some criteria, such as dexterity, isotropy, velocity, payload capability and stiffness could be involved. This section will give the definition of some indices and the corresponding atlases. Practically, which criterion should be considered depends on the application situation and the designer's desirability.

[2] The MIC is defined as the circle that is located at the y-axis and is tangent with singular loci. It is used to measure the thickness of the workspace [19].

2.1. Global conditioning index (GCI) and its atlas

The velocity equation of the mechanism studied here can be written as

$$\dot{\boldsymbol{\theta}} = \boldsymbol{J}\dot{\boldsymbol{p}} \tag{1}$$

where $\dot{\boldsymbol{p}} = (\dot{y} \quad \dot{z})^{\mathrm{T}}$ is the vector of output velocities and $\dot{\boldsymbol{\theta}} = (\dot{\theta}_1 \quad \dot{\theta}_2)^{\mathrm{T}}$ is the vector of input velocities. From Eq. (1), one can derive [1]

$$\|\delta\dot{\boldsymbol{\theta}}\|/\|\dot{\boldsymbol{\theta}}\| \leqslant \kappa_J \|\delta\dot{\boldsymbol{p}}\|/\|\dot{\boldsymbol{p}}\| \tag{2}$$

where κ_J is the condition number of the matrix $\boldsymbol{J}$. Here, the 2-norm condition number is used. That is

$$\kappa_J = \sigma_1/\sigma_s, \quad \kappa_J \geqslant 1 \tag{3}$$

in which σ_1 and σ_s are the maximum and minimum singular values of $\boldsymbol{J}$. Then, from Eq. (2), mathematically, the condition number of a matrix can be used in numerical analysis to estimate the error generated in the solution of a linear system of equations by the error on the data. When applied to the Jacobian matrix, the condition number will give a measure of the accuracy of the control of the mechanism. It can be also used to evaluate the dexterity and isotropy of a mechanism. This number is to be kept as small as possible. If the number can be unity, the matrix is an isotropic one, and the mechanism is in an isotropic configuration.

The condition number κ_J is configuration-dependent. Its reciprocal $1/\kappa_J$ ($0 \leqslant 1/\kappa_J \leqslant 1$) is a local performance index that is referred to as the *local conditioning index* (LCI). In order to evaluate the global behavior of a mechanism on a workspace, a global index can be defined as [9]

$$\eta_J = \int_W 1/\kappa_J \mathrm{d}W \Big/ \int_W \mathrm{d}W \tag{4}$$

which is the *global conditioning index* (GCI). In Eq. (4), W is the workspace of the mechanism. In particular, a large value of the index ensures that the mechanism can be precisely controlled.

For the mechanism studied here, the workspace W in Eq. (4) can be the MIW. The relationship between the GCI and the three normalized parameters $r_i (r_i = R_i/D,\ D = (R_1 + R_2 + R_3)/3$, and $i = 1, 2, 3)$ can be studied in the design space established in Ref. [19]. The corresponding atlas is shown in Fig. 2. To plot the atlas of Fig. 2, one should first calculate every GCI value of each non-dimensional mechanism with r_1, r_2 and r_3, which is included in the design space. Using Eq. (33) in Ref. [19], one can then obtain the relationship between the GCI and the two orthogonal coordinates s and t (see Fig. 9(b) in [19]). This relationship is practically used to plot the atlas in the planar system with s and t. The subsequent atlases are also plotted using the same method. Fig. 2 shows not only the relationship between the GCI and the two orthogonal coordinates but that between the GCI and the three non-dimensional parameters as well. What we really are most concerned about is the later relationship, for which s and t are not appeared in the figure.

From Fig. 2 one can see that:

- The line $r_1 + r_3 = r_2$ divides the design space into two parts.
- In the right part, if r_1 is specified the GCI value is inverse proportional to r_3.

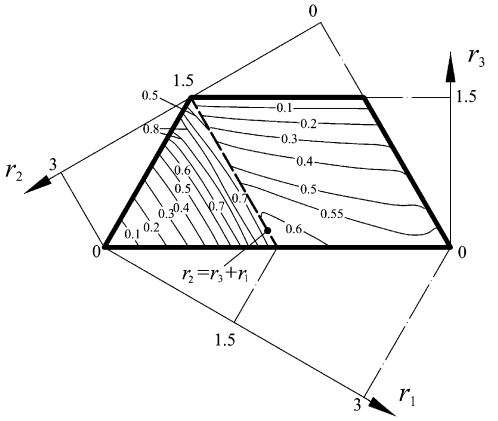

Fig. 2. Atlas of the global conditioning index.

- The mechanism with best GCI is in the left part. In the region where $r_2 \in [1.56, 1.9]$, the GCI is better, GCI > 0.6.

Fig. 3 gives the atlas of the *maximum conditioning index* (MCI) of the mechanism. The MCI is defined as the maximum LCI in the MIW. As mentioned above, if the LCI is unity the mechanism is in the isotropy configuration. From Fig. 3, if one wants to find an (near) isotropy mechanism, he can select the mechanism in the region where MCI > 0.995. Notably, according to the definition of the MCI, an isotropy mechanism is not isotropy at every point within the workspace. Actually, there is no such a mechanism.

2.2. Global velocity index (GVI) and its atlas

Eq. (1) can be rewritten as

$$\dot{\boldsymbol{p}} = \boldsymbol{J}^{-1}\dot{\boldsymbol{\theta}} \tag{5}$$

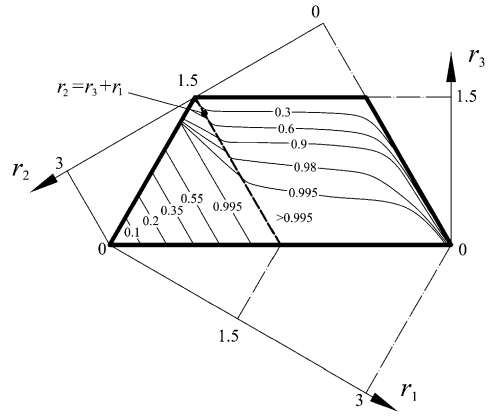

Fig. 3. Atlas of the maximum conditioning index.

from which one can write

$$\dot{\boldsymbol{p}}^{\mathrm{T}}\dot{\boldsymbol{p}} = \dot{\boldsymbol{\theta}}^{\mathrm{T}}\left(\boldsymbol{J}^{-1}\right)^{\mathrm{T}}\boldsymbol{J}^{-1}\dot{\boldsymbol{\theta}} \tag{6}$$

Let the input velocity vector $\dot{\boldsymbol{\theta}}$ be unit, i.e.,

$$\|\dot{\boldsymbol{\theta}}\|^2 = \dot{\boldsymbol{\theta}}^{\mathrm{T}}\dot{\boldsymbol{\theta}} = 1 \tag{7}$$

Under the condition (7), one can derive the extremum of the norm of vector $\dot{\boldsymbol{p}}$. In order to obtain the conditional extremum, using the Lagrange multiplier λ_V, one can construct the Lagrange equation as following:

$$L_V = \dot{\boldsymbol{\theta}}^{\mathrm{T}}\left(\boldsymbol{J}^{-1}\right)^{\mathrm{T}}\boldsymbol{J}^{-1}\dot{\boldsymbol{\theta}} - \lambda_V\left(\dot{\boldsymbol{\theta}}^{\mathrm{T}}\dot{\boldsymbol{\theta}} - 1\right) \tag{7a}$$

The necessary condition to the conditional extremum is

$$\left.\begin{aligned} \frac{\partial L_V}{\partial \lambda_V} &= 0 : \dot{\boldsymbol{\theta}}^{\mathrm{T}}\dot{\boldsymbol{\theta}} - 1 = 0 \\ \frac{\partial L_V}{\partial \dot{\boldsymbol{\theta}}} &= 0 : \left(\boldsymbol{J}^{-1}\right)^{\mathrm{T}}\boldsymbol{J}^{-1}\dot{\boldsymbol{\theta}} - \lambda_V\dot{\boldsymbol{\theta}} = 0 \end{aligned}\right\} \tag{8}$$

from which one can see that the Lagrange multiplier λ_V is actually the eigenvalue of matrix $(\boldsymbol{J}^{-1})^{\mathrm{T}}\boldsymbol{J}^{-1}$. Then, the norm of vector $\dot{\boldsymbol{p}}$ can be written as

$$\|\dot{\boldsymbol{p}}\|^2 = \dot{\boldsymbol{p}}^{\mathrm{T}}\dot{\boldsymbol{p}} = \dot{\boldsymbol{\theta}}^{\mathrm{T}}\left(\boldsymbol{J}^{-1}\right)^{\mathrm{T}}\boldsymbol{J}^{-1}\dot{\boldsymbol{\theta}} = \dot{\boldsymbol{\theta}}^{\mathrm{T}}\lambda_V\dot{\boldsymbol{\theta}} = \lambda_V \tag{9}$$

Therefore, the extremum of $\|\dot{\boldsymbol{p}}\|^2$ is the extremum of the eigenvalue of the matrix $(\boldsymbol{J}^{-1})^{\mathrm{T}}\boldsymbol{J}^{-1}$. Then, when the input velocity vector is unit, the maximum and minimum output velocities of the mechanism could be described as

$$\|\boldsymbol{V}_{\max}\| = \sqrt{\max\left(|\lambda_{Vi}|\right)} \quad \text{and} \quad \|\boldsymbol{V}_{\min}\| = \sqrt{\min\left(|\lambda_{Vi}|\right)} \tag{10}$$

where λ_{Vi} ($i = 1, 2$) are the eigenvalues of the matrix $(\boldsymbol{J}^{-1})^{\mathrm{T}}\boldsymbol{J}^{-1}$. The maximum and minimum output velocities form a velocity ellipsoid, whose axes lie in the directions of the eigenvectors of the matrix $(\boldsymbol{J}^{-1})^{\mathrm{T}}\boldsymbol{J}^{-1}$. Its magnitudes are the maximum and minimum output velocities given by Eq. (10). The mechanism can output a maximum (minimum) velocity in the direction of the major (minor) axis of the ellipsoid. Since the ellipsoid is calculated from the input velocity satisfying Eq. (7), the larger its volume is, the larger the output velocity is.

Since the Jacobian matrix is depended on the pose of a mechanism, the maximum and minimum output velocities are also configuration-dependent. The velocity index given by Eq. (10) can be only used to evaluate the velocity performance of a mechanism in a specified pose. For such a reason, here a global velocity index is defined as following:

$$\eta_{V\max} = \int_W \|\boldsymbol{V}_{\max}\|\mathrm{d}W \Big/ \int_W \mathrm{d}W \quad \text{and} \quad \eta_{V\min} = \int_W \|\boldsymbol{V}_{\min}\|\mathrm{d}W \Big/ \int_w \mathrm{d}W \tag{11}$$

where W is the workspace of the mechanism. For the mechanism studied here, W is a circular workspace with the radius of $r_{\mathrm{MIC}}/2$ (the reason will be given in Section 3.2.2).

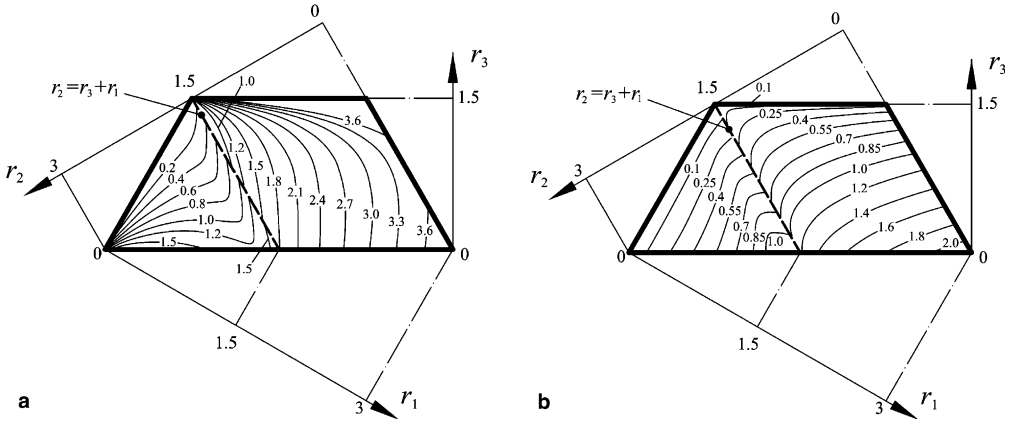

Fig. 4. Atlas of the GVI: (a) the atlas of $\eta_{V\max}$; (b) the atlas of $\eta_{V\min}$.

Fig. 4(a) and (b) show the atlases of $\eta_{V\max}$ and $\eta_{V\min}$, respectively, from which one can see that:

- The line $r_1 + r_3 = r_2$ divides the design space into two parts.
- In the right part of the atlas for $\eta_{V\max}$, if r_3 is specified the $\eta_{V\max}$ value is proportional to r_1.
- In the right part of the atlas for $\eta_{V\min}$, if r_2 is specified the $\eta_{V\min}$ value is proportional to r_1.
- In the left parts of the atlases for both $\eta_{V\max}$ and $\eta_{V\min}$, if r_2 is specified the $\eta_{V\max}$ and $\eta_{V\min}$ values are proportional to r_1.
- All in all, if r_3 is specified, a longer r_1 can lead to larger $\eta_{V\max}$ and $\eta_{V\min}$, i.e., better GVI performance. This is obvious. Practically, compared with a mechanism with parameters r_1, r_2 and r_3 ($0 < r_1, r_2 < 3$ and $0 \leqslant r_3 \leqslant 1.5$), a single-link mechanism with $r_3 = 3.0$ ($r_1 = r_2 = 0$) can output a largest velocity.

2.3. Global payload index (GPI) and its atlas

Payload capability is one of the most important performance indices of the parallel mechanism. It determines whether the mechanism can support the external force acting on the moving platform or not.

By virtue of what is called the *duality of kinematic and static* [20], the forces and moments applied at the moving platform under static conditions are related to the forces or moments required at the actuators to maintain the equilibrium by the transpose of the Jacobian matrix $\boldsymbol{J}$. We can write

$$\boldsymbol{\tau} = \boldsymbol{J}^{\mathrm{T}}\boldsymbol{f} \tag{12}$$

where $\boldsymbol{f}$ is the vector of actuator forces or torques, and $\boldsymbol{\tau}$ is the generalized vector of Cartesian forces and torques at the moving platform. Supposing that the vector $\boldsymbol{f}$ is unity, using the Lagrange equation with the multiplier λ_F, we can also obtain the extremum of the norm of vector $\boldsymbol{\tau}$, that is

$$\|\boldsymbol{\tau}_{\max}\| = \sqrt{\max\left(|\lambda_{Fi}|\right)} \quad \text{and} \quad \|\boldsymbol{\tau}_{\min}\| = \sqrt{\min\left(|\lambda_{Fi}|\right)} \tag{13}$$

where λ_{Fi} ($i = 1, 2$) are the eigenvalues of the matrix $\boldsymbol{J}\boldsymbol{J}^{\mathrm{T}}$. $\|\boldsymbol{\tau}_{\max}\|$ and $\|\boldsymbol{\tau}_{\min}\|$ are actually the maximum and minimum external forces that the mechanism can stand when the input force vector is unity. The maximum and minimum forces form a force ellipsoid, whose axes lie in the directions of the eigenvectors of the matrix $\boldsymbol{J}\boldsymbol{J}^{\mathrm{T}}$. Its magnitudes are the maximum and minimum external forces given by Eq. (13). The mechanism can stand a maximum (minimum) external force in the direction of the major (minor) axis of the ellipsoid. The larger its volume is, the larger the payload capability is.

Since the Jacobian matrix is depended on the pose of a mechanism, the maximum and minimum external forces given by Eq. (13) are also configuration-dependent. Based on the maximum and minimum external forces, a *global payload index* that can evaluate the payload capability within the workspace can be defined as

$$\eta_{F\max} = \int_W \|\boldsymbol{\tau}_{\max}\| \mathrm{d}W \Big/ \int_W \mathrm{d}W \quad \text{and} \quad \eta_{F\min} = \int_W \|\boldsymbol{\tau}_{\min}\| \mathrm{d}W \Big/ \int_w \mathrm{d}W \tag{14}$$

where W is the workspace of the mechanism. For the mechanism studied here, W is a circular workspace with the radius of $r_{\mathrm{MIC}}/2$. Considering the safety of a device, $\eta_{F\min}$ is usually used as the criterion to design the mechanism with respect to the payload capability.

Fig. 5(a) and (b) show the atlases of $\eta_{F\max}$ and $\eta_{F\min}$, respectively. From the atlases one can see that:

- The line $r_1 + r_3 = r_2$ divides the design space into two parts.
- In the right part of the atlas for $\eta_{F\max}$, if r_2 is specified the $\eta_{F\min}$ value is proportional to r_3 or inverse proportional to r_1.
- In the right part of the atlas for $\eta_{F\min}$, if r_3 is specified the $\eta_{F\min}$ value is proportional to r_2 or inverse proportional to r_1.
- In the left parts of the atlases for both $\eta_{F\max}$ and $\eta_{F\min}$, if r_2 is specified the $\eta_{F\max}$ and $\eta_{F\min}$ values are inverse proportional to r_1.
- All in all, if r_3 is specified, a smaller r_1 can lead to larger $\eta_{F\max}$ and $\eta_{F\min}$, i.e., better GPI performance. This is what it should be. One can imagine that if the input moment is locked the

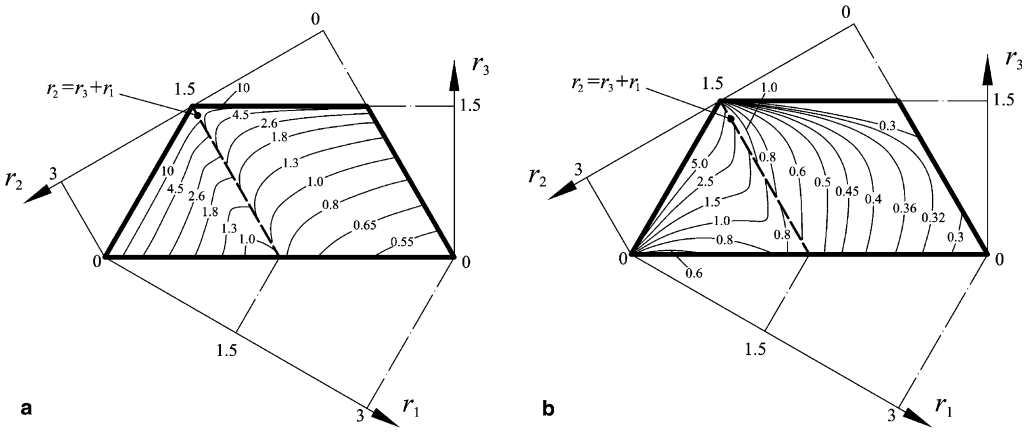

Fig. 5. Atlas of the GPI: (a) the atlas of $\eta_{F\max}$; (b) the atlas of $\eta_{F\min}$.

shorter the moment arm is the larger the force to balance the system will be. This also matches the Lever Law.

- Comparing Fig. 4 with Fig. 5, one can see that the distribution of GVI is almost contrary to that of GPI. The reason can be traced to the matrix $\boldsymbol{J}$ and the definition of these two indices. Observing Eqs. (10) and (13), it is not difficult to find that $\max(|\lambda_{Fi}|) = 1/\min(|\lambda_{Vi}|)$ and $\min(|\lambda_{Fi}|) = 1/\max(|\lambda_{Vi}|)$. That means the maximum (minimum) external force given in Eq. (13) is actually the inverse of the minimum (maximum) output velocity in Eq. (10).

2.4. Global stiffness index (GSI) and its atlas

There will be deformation on the end-effector if the external force acts on it. The deformation is depended on the mechanism stiffness and the external force. The mechanism stiffness affects the dynamics and the position accuracy of the device, for which stiffness is an important performance index. Especially, the static stiffness (or rigidity) of the mechanism can be a primary consideration in the design of a parallel mechanism for certain applications, e.g., machine tools.

In the operational coordinate space, we define a stiffness matrix $\boldsymbol{K}$ that relates the external force vector $\boldsymbol{\tau}$ at the moving platform to the output displacement vector $\boldsymbol{D}$ of the moving platform according to

$$\boldsymbol{D} = \boldsymbol{K}^{-1}\boldsymbol{\tau} \tag{15}$$

where the stiffness matrix $\boldsymbol{K}$ is expressed as

$$\boldsymbol{K} = \boldsymbol{J}^{\mathrm{T}}\boldsymbol{K}_p\boldsymbol{J} \tag{16}$$

with

$$\boldsymbol{K}_p = \begin{bmatrix} k_{p1} & \\ & k_{p2} \end{bmatrix} \tag{17}$$

in which k_{pi} is a scalar representing the stiffness of each of the actuators.

If $k_{p1} = k_{p2} = 1$ and $\|\boldsymbol{\tau}\|^2 = 1$, the maximum and minimum deformations can be obtained as

$$\|\boldsymbol{D}_{\max}\| = \sqrt{\max(|\lambda_{Di}|)} \quad \text{and} \quad \|\boldsymbol{D}_{\min}\| = \sqrt{\min(|\lambda_{Di}|)} \tag{18}$$

where λ_{Di} ($i = 1, 2$) are the eigenvalues of the matrix $(\boldsymbol{K}^{-1})^{\mathrm{T}}\boldsymbol{K}^{-1}$. $\|\boldsymbol{D}_{\max}\|$ and $\|\boldsymbol{D}_{\min}\|$ are actually the maximum and minimum deformations on the end-effector when both the external force vector and the matrix $\boldsymbol{K}_p$ are unity. The maximum and minimum deformations form a deformation ellipsoid, whose axes lie in the directions of the eigenvectors of the matrix $(\boldsymbol{K}^{-1})^{\mathrm{T}}\boldsymbol{K}^{-1}$. Its magnitudes are the maximum and minimum deformations given by Eq. (18). The end-effector of the mechanism can yield a maximum (minimum) external deformation in the direction of the major (minor) axis of the ellipsoid. The smaller its volume is, the better the stiffness is.

Similarly, based on Eq. (18), the *global stiffness index* that can evaluate the stiffness of a mechanism within the workspace is defined as

$$\eta_{D\max} = \int_W \|\boldsymbol{D}_{\max}\| \mathrm{d}W \Big/ \int_W \mathrm{d}W \quad \text{and} \quad \eta_{D\min} = \int_W \|\boldsymbol{D}_{\min}\| \mathrm{d}W \Big/ \int_W \mathrm{d}W \tag{19}$$

where, for the mechanism studied here, W is a circular workspace with the radius of $r_{\mathrm{MIC}}/2$. Usually, $\eta_{D\max}$ can be used as the criterion to design the mechanism with respect to the stiffness. Normally, we expect the index value to be as small as possible.

Fig. 6(a) and (b) show the atlases of $\eta_{D\max}$ and $\eta_{D\min}$, respectively, from which one can see that:

- The distribution of the index in the design space is similar to that of the GVI.
- The line $r_1 + r_3 = r_2$ divides the design space into two parts.
- In the right part of the atlas for $\eta_{D\max}$, if r_3 is specified the $\eta_{D\max}$ value is proportional to r_1.
- In the right part of the atlas for $\eta_{D\min}$, if r_2 is specified the $\eta_{D\min}$ value is proportional to r_1.
- In the left parts of the atlases for both $\eta_{D\max}$ and $\eta_{D\min}$, if r_2 is specified the $\eta_{D\max}$ and $\eta_{D\min}$ values are proportional to r_1.
- All in all, if r_3 is specified, a longer r_1 leads to larger $\eta_{D\max}$ and $\eta_{D\min}$, i.e., worse stiffness performance.
- From Fig. 6, we can see that in the region where $r_1 + r_3 < r_2$, the stiffness of a mechanism will be better. And a shorter r_1 can make a mechanism better stiffness. Especially, when $r_1 = 0$, the stiffness of a mechanism will be best. Actually, $r_1 = 0$ results in a triangle mechanism, which is best in stability.
- From Fig. 6, one can also conclude that the stiffness of a mechanism with $r_3 = 1.5$ ($r_3 = r_1 + r_2$) can be worst along one direction and best along another direction. The mechanism with $r_3 = r_1 + r_2$ is such a mechanism that the five bars are collinear. It can be assembled and cannot move. If an external force is acted on the end-effector point P along the direction from A_1 (A_2) to A_2 (A_1), the deformation is smallest. Along the direction normal to A_1A_2, the deformation is undoubtedly largest.
- Since $\max(|\lambda_{Di}|)$ and $\min(|\lambda_{Di}|)$ are always proportional to $\max(|\lambda_{Vi}|)$ and $\min(|\lambda_{Vi}|)$, respectively. The stiffness is always inconsistent with the velocity performance. Figs. 4 and 6 show the fact.

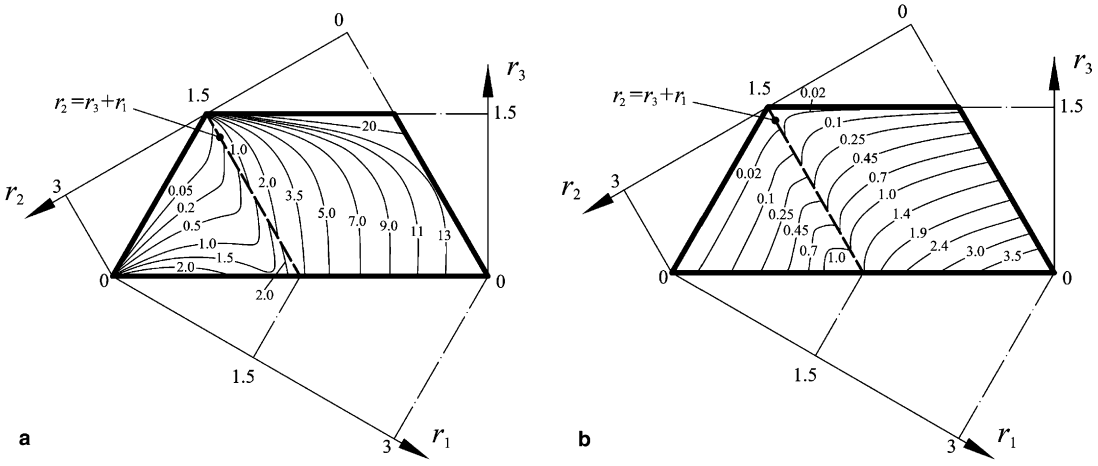

Fig. 6. Atlas of the GSI: (a) the atlas of $\eta_{D\max}$; (b) the atlas of $\eta_{D\min}$.

3. Optimum design example based on the atlas

3.1. Optimum region with respect to desired performances

The relationships between performance indices and the link lengths of the planar 5R parallel mechanism have been studied. The results have been illustrated by their atlases, from which one can visually know which mechanism can be with a better performance and which cannot. This is very important for us to find out a global optimum mechanism for a specified application. In this section, the optimum region will be shown first with respect to possible performances.

3.1.1. Workspace and GCI

In almost all designs, the workspace and GCI are usually considered. From the atlas of the MIC radius (see Fig. 19 in Ref. [19]) and the distribution chart of MIC in the design space (Fig. 18 in Ref. [19]), we can see that the workspace of a mechanism in sub-regions IVa, IVb, Va and Vb can be larger. From the atlas of GCI (Fig. 2), we know that the mechanism when $r_2 \in [1.56, 1.9]$ can have better GCI. If the MIC radius, denoted as r_{MIC}, is supposed to be greater than 0.8 ($r_{\mathrm{MIC}} > 0.8$) and the GCI greater than 0.6, the optimum region in the design space can be obtained as shown in Fig. 7(a). The region is denoted as $\Omega_{W\text{–}\mathrm{GCI}} = [(r_1, r_2, r_3) | r_{\mathrm{MIC}} > 0.8$ and $\eta_J > 0.6]$ with performance restriction. One can also obtain an optimum region with better workspace and GCI, for example, the region $\Omega'_{W\text{–}GCI}$ where $r_{\mathrm{MIC}} > 1.0$ and $\eta_J > 0.7$ as shown in Fig. 7(b). In order to get a better result, one can decrease the optimum region with stricter restriction. Such a region contains all possible optimum results.

After the optimum region is identified, there are two ways to achieve the optimum design result with non-dimensional parameters. One is to search a most optimal result within the region $\Omega_{W\text{–}\mathrm{GCI}}$ or $\Omega'_{W\text{–}GCI}$ using one classical searching algorithm based on an established object function. The method will yield a unique solution. This is not the content of this paper. Another one is to select a mechanism within the obtained optimum region. For example, the mechanism with $r_1 = 1.1$, $r_2 = 1.65$ and $r_3 = 0.25$ can be selected as the candidate if only workspace and GCI are involved

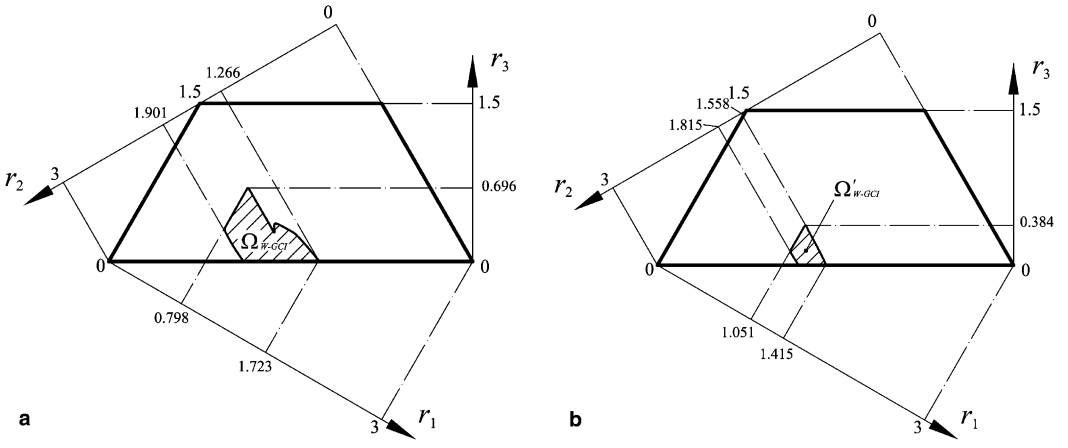

Fig. 7. The optimum region with specified MIC and good GCI.

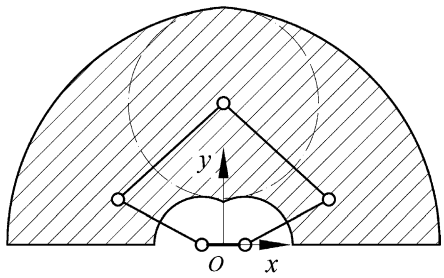

Fig. 8. One example in the optimum region $\Omega'_{W\text{–}GCI}$.

in the design. Its MIC radius and the GCI are $r_{\mathrm{MIC}} = 1.1$ and 0.7929, respectively. Because $r_2 > r_1 + r_3$ and $r_1 > r_3$, the mechanism is in the sub-region IVa. There is no the singularity that the points B_1, P and B_2 are collinear in the workspace. The mechanism and its workspace are shown in Fig. 8. The advantage of the later method is that the designer can adjust the design result fitly trying to select another candidate in the optimum region.

3.1.2. Workspace, GCI, and GVI

Considering the velocity performance, from Fig. 4, one can see that the mechanisms in sub-regions IIIb, IVb and Vb can be the candidates. Especially, the mechanisms in sub-region IVb have better velocity performance. In some application cases, if velocity is most important, one can select a mechanism from sub-region IVb. Mostly, at such cases, the workspace should be large enough and the GCI should be good as well. For example, an optimum region $\Omega_{W\text{–GCI–GVI}} = [(r_1, r_2, r_3) | r_{\mathrm{MIC}}(r_1, r_2, r_3) > 0.6, \eta_J > 0.55, \eta_{V\min} > 1.0$ and $\eta_{V\max} > 1.5]$ can be identified as shown in Fig. 9 if these three indices are all considered. The non-dimensional parameters of one mechanism within the region are $r_1 = 1.5$, $r_2 = 1.2$ and $r_3 = 0.3$. Its indices are $r_{\mathrm{MIC}} = 0.7385$, $\eta_J = 0.5853$, $\eta_{V\max} = 2.0745$ and $\eta_{V\min} = 1.2389$, respectively. Because $r_1 = r_2 + r_3$, there is the singularity that the points B_1, P and B_2 are collinear in its workspace. The mechanism and its workspace are shown in Fig. 10.

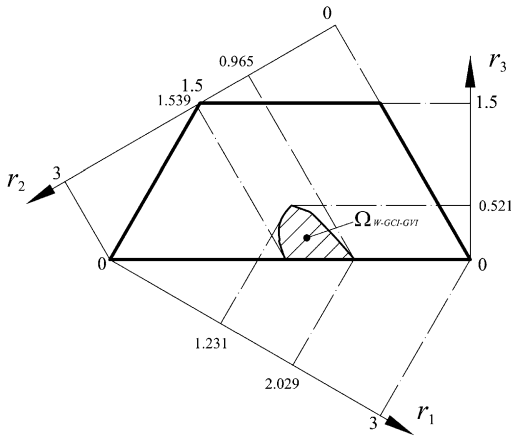

Fig. 9. An optimum region with specified MIC, GVI and good GCI.

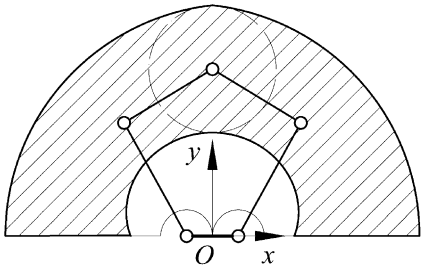

Fig. 10. One example in the optimum region $\Omega_{W\text{–GCI–GVI}}$.

3.1.3. Workspace, GCI, and GPI

From Fig. 5, we can see that the payload capability of the mechanisms in sub-regions IIa and IIIa is very good. Since some mechanisms in sub-region IIIa have very good GCI performance, if only GPI and GCI are involved in the design (for example, in the application of micro-manipulator), one can select a mechanism from sub-region IIIa.

From the MIC related atlases presented in Ref. [19], one can notice that the workspace performance of the mechanisms in sub-regions IIa and IIIa is not good. Considering the workspace, GCI and GPI, simultaneously, one optimum region $\Omega_{W\text{–GCI–GPI}} = [(r_1, r_2, r_3)|r_{\text{MIC}}(r_1, r_2, r_3) > 0.6, \eta_J > 0.6, \eta_{F\min} > 1.2$ and $\eta_{F\max} > 1.5]$ can be obtained as shown in Fig. 11. One example within the region is that with $r_1 = 0.7$, $r_2 = 1.7$ and $r_3 = 0.6$. Its indices are $r_{\text{MIC}} = 0.75$, $\eta_J = 0.7961$, $\eta_{F\max} = 1.5605$ and $\eta_{F\min} = 1.4253$, respectively. Because $r_2 > r_1 + r_3$ and $r_1 > r_3$, the mechanism is in the sub-region IVa. There is no the singularity that the points B_1, P and B_2 are collinear. The mechanism and its workspace are shown in Fig. 12.

3.1.4. Workspace, GCI, and GSI

Because a mechanism with smaller $\eta_{D\max}$ and $\eta_{D\min}$ values usually has better stiffness, the mechanisms in sub-regions IIIa and IVa, where $r_2 > r_1 + r_3$, are better in the performance. Some mechanisms in sub-region IIIa are very good in both the stiffness and GCI but bad in workspace. These

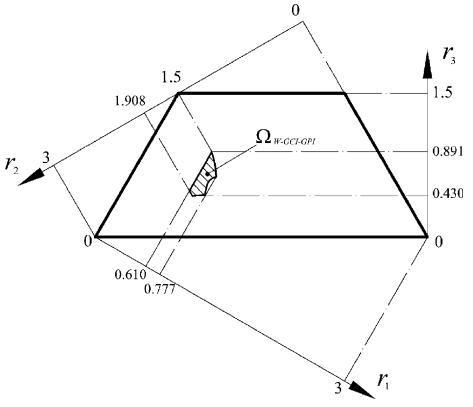

Fig. 11. An optimum region with specified MIC, GPI and good GCI.

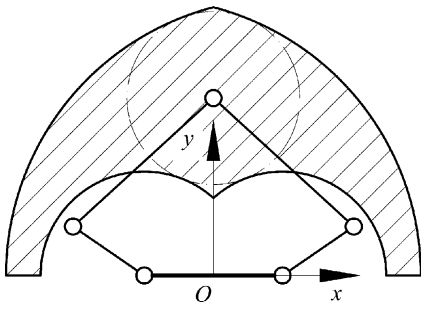

Fig. 12. One example in the optimum region $\Omega_{W\text{–GCI–GPI}}$.

mechanisms can be applied in the field where small workspace is needed. If the workspace, conditioning index and stiffness should be all considered in the design, the mechanism can be selected from an optimum region $\Omega_{W\text{–GCI–GSI}} = [(r_1, r_2, r_3)|r_{\text{MIC}}(r_1, r_2, r_3) > 0.7, \eta_J > 0.6, \eta_{D\min} < 0.7$ and $\eta_{D\max} < 1.0]$, as shown in Fig. 13. The non-dimensional parameters of one example within the region are $r_1 = 0.85$, $r_2 = 1.6$ and $r_3 = 0.55$. Its indices are $r_{\text{MIC}} = 0.85$, $\eta_J = 0.7509$, $\eta_{D\max} = 0.8133$ and $\eta_{D\min} = 0.\ 5475$, respectively. Because the mechanism is in the sub-region IVa, there is no the

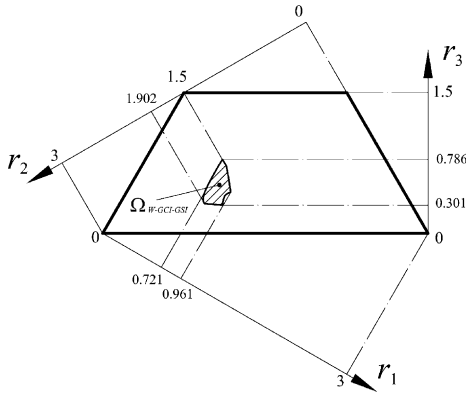

Fig. 13. An optimum region with specified MIC, GSI and good GCI.

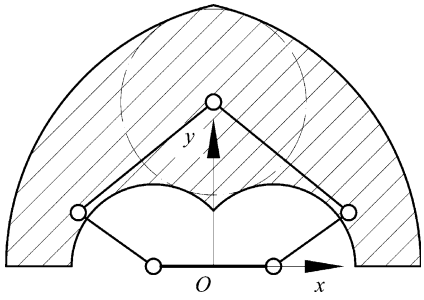

Fig. 14. One example in the optimum region $\Omega_{W\text{–GCI–GSI}}$.

singularity that the points B_1, P and B_2 are collinear. Fig. 14 shows the mechanism and its workspace.

3.1.5. Workspace, GCI, GVI, GPI and GSI

In most designs, we should not consider all these performances. Here, this is only an example to present an optimum region for this case. If the indices are specified as $r_{\mathrm{MIC}} > 0.85$, $\eta_J > 0.58$, $\eta_{V\max} > 1.2$, $\eta_{V\min} > 0.85$, $\eta_{F\max} > 1.0$, $\eta_{F\min} > 0.6$, $\eta_{D\max} < 2.85$ and $\eta_{D\min} < 1.2$, the optimum region Ω_{All} can be obtained as shown in Fig. 15.

The non-dimensional parameters of an example within the region are $r_1 = 1.17$, $r_2 = 1.45$ and $r_3 = 0.38$. Its indices are $r_{\mathrm{MIC}} = 1.05$, $\eta_J = 0.5971$, $\eta_{V\max} = 1.5378$, $\eta_{V\min} = 0.9212$, $\eta_{F\max} = 1.1041$, $\eta_{F\min} = 0.6592$, $\eta_{D\max} = 2.4045$ and $\eta_{D\min} = 0.8595$, respectively. Because $r_2 < r_1 + r_3$, $r_2 > r_1$ and $r_1 > r_3$, the mechanism is from the sub-region Va. In its workspace, there is the singularity that the points B_1, P and B_2 are collinear. The mechanism and its workspace are shown in Fig. 16.

In Section 3.1, some optimum examples have been given with respect to specified performance indices. The constraints on the indices have no special technical meanings. They are used to guarantee the intersection (the optimum region) of different atlases and make the intersection suitable in area. Notably, these optimum regions can be changed with respect to the design specification and designer's requirements, as shown in Section 3.1.1. The optimum examples obtained in this

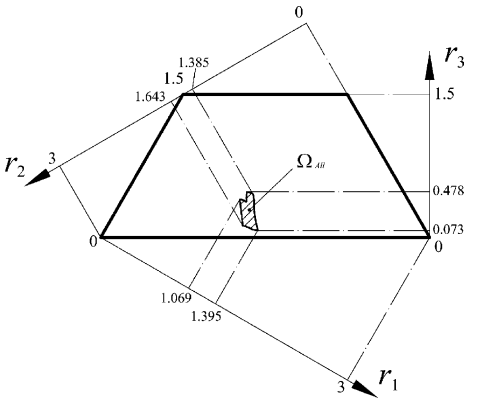

Fig. 15. An optimum region with specified MIC, GVI, GPI, GSI and good GCI.

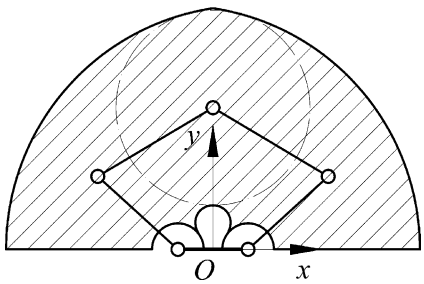

Fig. 16. One example in the optimum region Ω_{All}.

section are just used to show how to utilize the obtained performance charts in the optimum design process. Following the presented examples, it is not difficult to identify an optimum region that a designer wants. Although we can pick up a mechanism from one optimum region, it cannot be applied to practice yet because the mechanism is with non-dimensional parameters. Namely, this is not the final optimum result.

3.2. Dimension determination

The final objective of optimum design is to determine the link lengths of a mechanism. In the last section, some optimum regions in the design space have been presented as examples. These regions consist of mechanisms with non-dimensional parameters. The selected optimum mechanisms with non-dimension are comparative results. They are not the final optimum design results. Their workspaces are maybe so small that cannot be used practically. What is more, the defined MIW still consists of singular points. In the design process, the points where the desired indices are bad should be excluded from the workspace. In this section, a desired workspace will be given beforehand. The link lengths of a mechanism that can work within this workspace with better (best) performances will be determined.

3.2.1. Explanation on two terms: usable workspace and maximal inscribed workspace

Here, before to present the dimension determination of a mechanism, we would like to explain the reasonability of the definition and application of two terms. Firstly, it is about the *usable workspace*. In Ref. [19], we defined one singularity-free region that is above the x-axis as the *usable workspace*. According to the definition in Ref. [19], a usable workspace is not the workspace that can be used in practical by a device. Actually, only part of the usable workspace can be available for a device. The workspace can be referred to as the *practical workspace* or *good-conditioning workspace* (GCW), which can be restricted by the control accuracy index, i.e., the local conditioning index (LCI). The specified index value can be determined by the designer. Fig. 17 shows the distribution of the LCI on the whole singularity-free workspace of the mechanism with $r_1 = 0.85$, $r_2 = 1.6$ and $r_3 = 0.55$. From the figure, one can see that the LCI within the region where $x < 0.0$ is worse. That means if the region restricted by $1/\kappa_J = 0.5$ is considered as the GCW, the space when $x < 0.0$ will not be included. Actually, most mechanisms (except those with $r_3 = 0$) in sub-regions IVa and Va have the similar characteristic. For the mechanisms in sub-regions IVb, and Vb, although there are two or more good-conditioning regions, they are separated by points with worse LCIs. Then, the usable workspace defined as the region where $x > 0.0$ in Ref. [19] is closer to the practical workspace than the whole workspace.

Secondly, it is about the importance of the MIW. In Ref. [19], we presented the atlas of the MIC radius instead of the usable workspace. In this paper, the global indices are also defined with respect to the MIW not the usable workspace. To explain this, let's check out two 5R parallel mechanisms. The first one is that with the parameters $r_1 = 0.4$, $r_2 = 2.33$ and $r_3 = 0.27$, whose usable workspace with the area of 3.3453 is shown in Fig. 18(a). Its MIC radius is $r_{\mathrm{MIC}} = 0.4$. The second one is that with parameters $r_1 = 0.65$, $r_2 = 1.62$ and $r_3 = 0.73$. Its usable workspace is shown in Fig. 18(b), and the area is 2.2390. The MIC radius is $r_{\mathrm{MIC}} = 0.65$. Then, the first mechanism has a larger usable workspace area than the second mechanism. But the MIC radius of the first mechanism is shorter than the second one. For the two mechanisms, the distribution of the

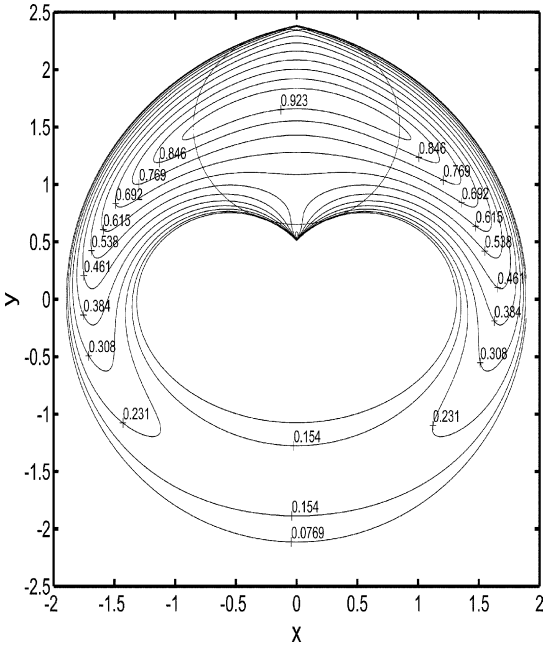

Fig. 17. The distribution example of LCI on the whole workspace.

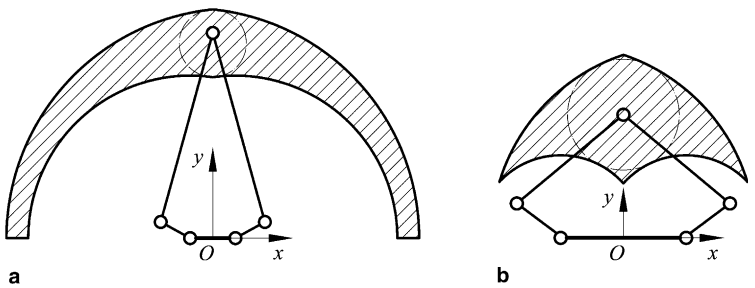

Fig. 18. The workspaces of two example mechanisms.

LCI on the usable workspace are shown in Fig. 19(a) and (b), respectively, from which it is not difficult to conclude that the GCW restricted by $1/\kappa_J = 0.5$ of the second mechanism is larger than that of the first one. Actually, there is no such a GCW for the first mechanism. Generally, a flatter workspace means the most points are far from the singular loci. And a thinner one means most points are near to the singularity. What we are concerned about is how useful the workspace is but not how large the area is. These two examples show that a larger usable workspace does not mean a larger GCW. But if the MIW is larger, the GCW will be larger as well. Therefore, the MIC or the MIW can characterize the workspace performance. That is the reason why we presented the atlas of the MIW and defined the global indices with respect to the workspace. Although the MIW is more useful, the usable workspace cannot be replaced and ignored. It should be our research object as well, since the final GCW of a real mechanism is part of the usable workspace.

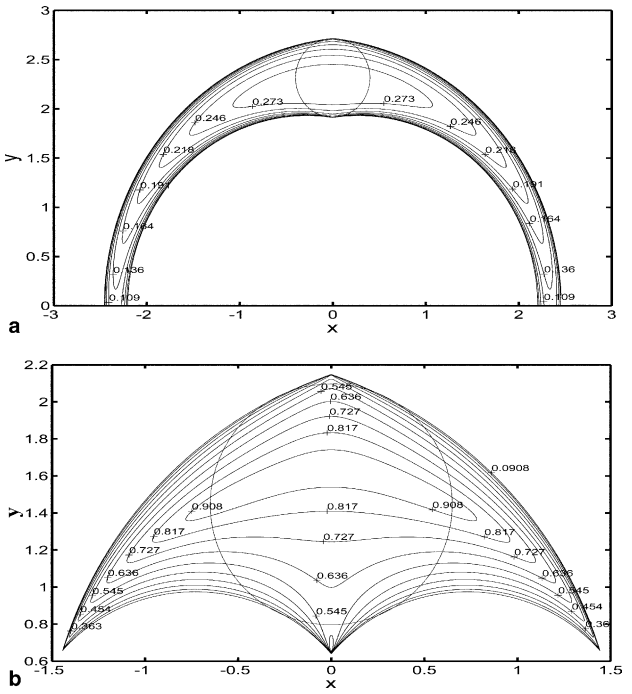

Fig. 19. LCI distribution for two comparative mechanisms: (a) the mechanism with a usable workspace area 3.3453; (b) the mechanism with a usable workspace area 2.2390.

Additionally, Figs. 17 and 19 show that the distribution of the LCI is continuous. The MIW includes all points with the LCI values from the minimum (zero) to the maximum. The point with the maximum (best) LCI is always within the MIW. Then, in Section 2.1 it is reasonable to search the MCI within the MIW. Due to such a continuous distribution, we can conclude that an index is good within the region near the MIW if it is good within it. This is also the reason why the MIW can be used as the reference to evaluate a performance globally.

3.2.2. Distribution of the performance indices in or near the singularity

As it is well known, in a singularity the Jacobian matrix is singular. The corresponding LCI should be zero. Fig. 20 shows the distribution of the LCI on the MIW of the mechanism with $r_1 = 1.1$, $r_2 = 1.65$ and $r_3 = 0.25$. From the figure, one can see that the LCI at the points of the usable workspace boundary is zero. For the example, there are four singular points, which are four tangent points between the MIC and the usable workspace boundary.

Singularity analysis (see Ref. [19]) shows that, in the stationary singularity, the non-zero input velocity vector $\dot{\boldsymbol{\theta}}$ will result the element of vector $\dot{\boldsymbol{p}}$ in zero. In this case, we can say that the end-effector loses one or more degrees of freedom. This implies that the end-effector can resist one or more forces or moments without exerting any torque or moment at the actuated joints. In another word, in such a singularity, the payload and stiffness of the mechanism will be very high. Fig. 21 shows the distribution of $\|\boldsymbol{V}_{\max}\|$, $\|\boldsymbol{\tau}_{\min}\|$ and $\|\boldsymbol{D}_{\max}\|$ on the workspace of the mechanism $r_1 = 1.5$, $r_2 = 1.2$ and $r_3 = 0.3$. The results show that near the stationary singularity the $\|\boldsymbol{V}_{\max}\|$ and $\|\boldsymbol{D}_{\max}\|$

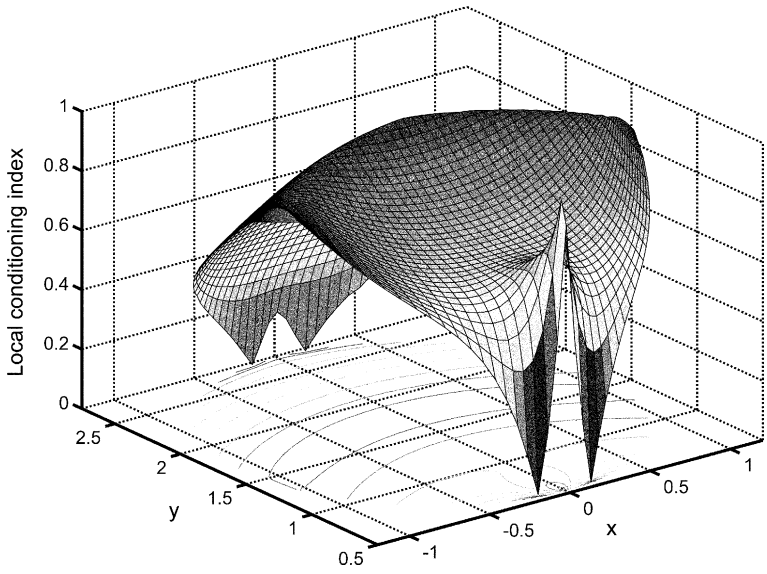

Fig. 20. Distribution of LCI on the MIW.

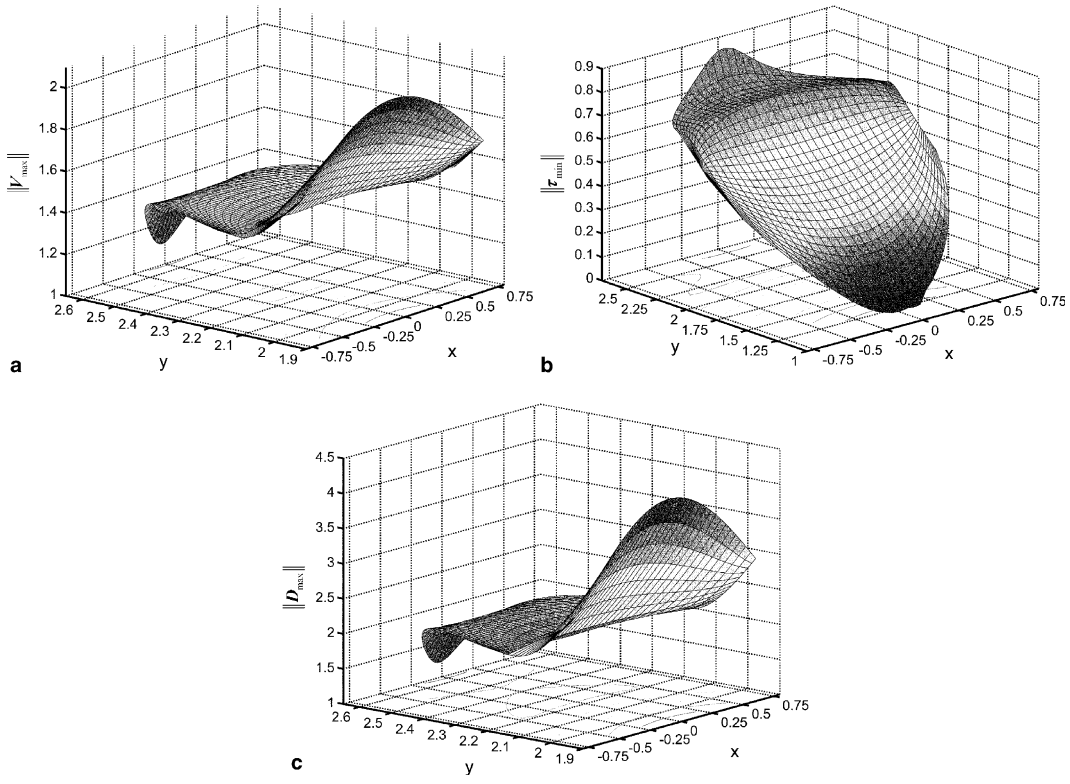

Fig. 21. Distribution of $\|\boldsymbol{V}_{\max}\|$, $\|\boldsymbol{\tau}_{\min}\|$ and $\|\boldsymbol{D}_{\max}\|$ on the workspace: (a) $\|\boldsymbol{V}_{\max}\|$ on half of MIW; (b) $\|\boldsymbol{\tau}_{\min}\|$ on MIW; (c) $\|\boldsymbol{D}_{\max}\|$ on half of MIW.

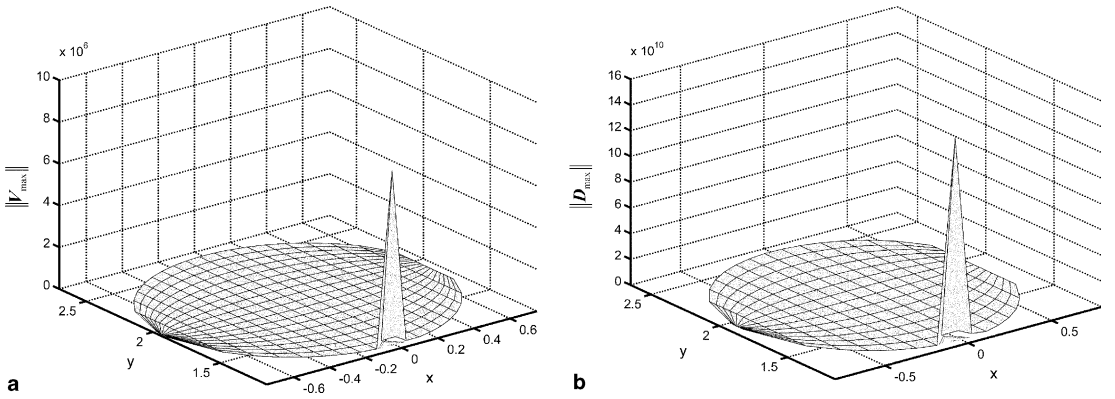

Fig. 22. Distribution of $\|\boldsymbol{V}_{\max}\|$ and $\|\boldsymbol{D}_{\max}\|$ on the MIW: (a) $\|\boldsymbol{V}_{\max}\|$; (b) $\|\boldsymbol{D}_{\max}\|$.

are small and $\|\boldsymbol{\tau}_{\min}\|$ is large. This means the velocity performance is bad and payload and stiffness are good.

In the uncertainty singularity, there exists non-zero vector $\dot{\boldsymbol{p}}$, which will correspond to a velocity of zero of the input joints. Then, the $\|\boldsymbol{V}_{\max}\|$ at the points of the uncertainty singular curve will be very large. In such a singularity, we can say that the end-effector gains one or more degrees of freedom. This implies that the end-effector cannot resist one or more forces or moments even when all actuators are locked. In another word, in this case, the payload and stiffness of the mechanism will be very poor. From Fig. 21(b), one can see that near the singularity $\|\boldsymbol{\tau}_{\min}\|$ value is small and the payload capability is poor. Fig. 22(a) and (b) show the distribution of $\|\boldsymbol{V}_{\max}\|$ and $\|\boldsymbol{D}_{\max}\|$ on the workspace for the mechanism $r_1 = 1.5$, $r_2 = 1.2$ and $r_3 = 0.3$ (There is the uncertainty singularity in its workspace). They show that near the uncertainty singularity the $\|\boldsymbol{V}_{\max}\|$ and $\|\boldsymbol{D}_{\max}\|$ are very large. This indicates that the velocity performance is good and stiffness is poor. The above analysis shows that the indices used and defined in this paper can evaluate the corresponding performances of the mechanism. They can be also applied to the performance evaluation of other parallel mechanisms.

In addition, notice that the local conditioning index $1/\kappa_J$ is no more than 1 and $1/\kappa_J = 0$ at a singular point. There are only four singular points in maximum within the MIW. The effect of such zero values to the final value of η_J is so little that can be ignored. Therefore, the whole MIW is used as the workspace to calculate the index η_J in Eq. (4). From Figs. 21 and 22, we can see that in some cases, especially in the singularities, the $\|\boldsymbol{V}_{\max}\|$, $\|\boldsymbol{V}_{\min}\|$, $\|\boldsymbol{\tau}_{\max}\|$, $\|\boldsymbol{\tau}_{\min}\|$, $\|\boldsymbol{D}_{\max}\|$ and $\|\boldsymbol{D}_{\min}\|$ values will be very large. They are sometimes so large that can affect the final global index values badly. Such a value will give us an incorrect result. We cannot predict such cases previously. For such reasons, a circular workspace with the radius of $r_{\mathrm{MIC}}/2$ is used as the workspace in Eqs. (11), (14) and (19).

3.2.3. Dimension determination based on the obtained optimum example

In Section 3.1, some optimum regions in the design space with involved performance indices are identified. One example for each optimum region is given. As an example to present how to determine the real dimensional parameters with respect to a non-dimensional optimum mechanism, we

consider the mechanism with $r_1 = 0.85$, $r_2 = 1.6$ and $r_3 = 0.55$ obtained in Section 3.1.4. The mechanism is from the optimum region $\Omega_{W\text{–GCI–GSI}}$, where the workspace, conditioning index and stiffness are involved in the design objective. The MIC radius of the mechanism is $r_{\text{MIC}} = 0.85$. As it was mentioned, the MIW consists of singular points and their neighborhoods, where the mechanism will be out of control. For the example, there is only the stationary singularity in its usable workspace. As shown in Fig. 23, the LCI is zero in singular points and very small near these points. However, the stiffness of the mechanism in these points is high as shown in Fig. 24. Therefore, in the process determining the dimensional parameters with respect to a desired workspace, the LCI can be the only performance to be considered.

The process to achieve the dimension of the non-dimensional optimum mechanism with respect to a desired workspace can be summarized as follows.

Step 1: To obtain the *good-conditioning workspace* (GCW) with a specified LCI. For example, if the LCI is given as $1/\kappa_J = 0.5$, the GCW of the mechanism bounded by the curve $\kappa_J = 0.5$ is shown

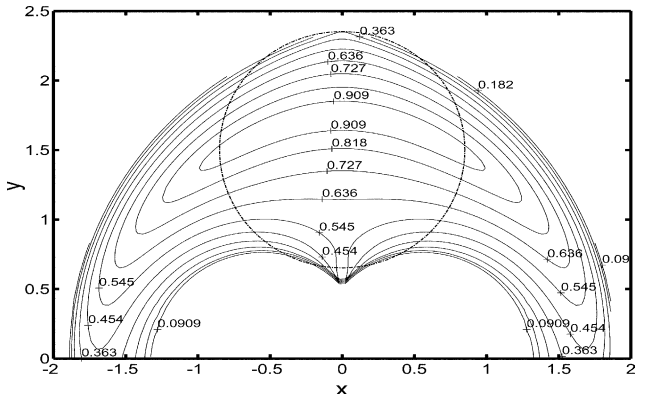

Fig. 23. The distribution of LCI on the usable workspace for the optimum mechanism with $r_1 = 0.85$, $r_2 = 1.6$ and $r_3 = 0.55$.

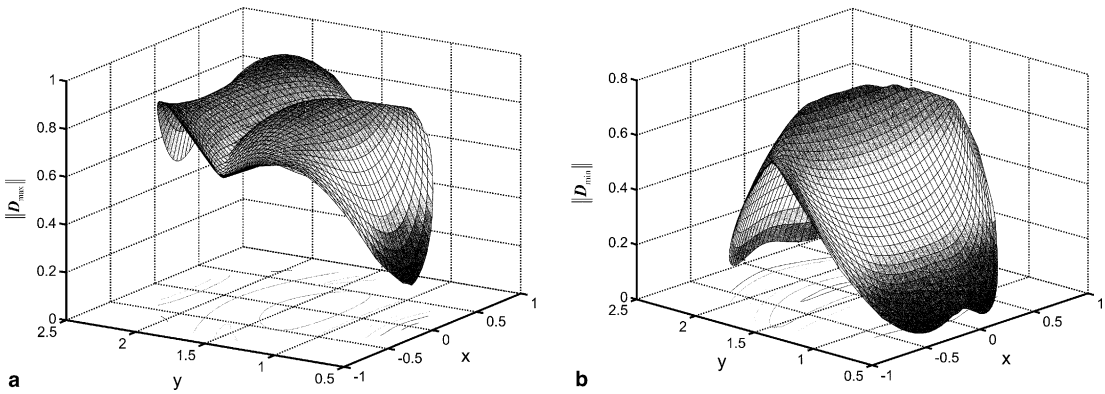

Fig. 24. Distribution of $\|\boldsymbol{D}_{\max}\|$ and $\|\boldsymbol{D}_{\min}\|$ on the MIW for the optimum mechanism with $r_1 = 0.85$, $r_2 = 1.6$ and $r_3 = 0.55$: (a) $\|\boldsymbol{D}_{\max}\|$; (b) $\|\boldsymbol{D}_{\min}\|$.

in Fig. 25. The area of the workspace is 3.4817. The GCI index within this workspace is $\eta_J = 0.6686$. Here, one can also check the stiffness performance. Fig. 26 shows the distribution of $\|\boldsymbol{D}_{\max}\|$ and $\|\boldsymbol{D}_{\min}\|$ on the workspace. With respect to this workspace, there are $\eta_{D\max} = 0.7656$ and $\eta_{D\min} = 0.3606$.

Step 2: To determine the dimensional factor D, which was used to change the dimensional geometric parameters of a mechanism to those with non-dimension. As analyzed in [19], the ratio of the workspace W_{Dim} of a dimensional mechanism to that $W_{\text{Non-Dim}}$ of a non-dimensional mechanism is D^2, that is

$$W_{\text{Dim}} = D^2 W_{\text{Non-Dim}} \tag{20}$$

The GCW of the non-dimensional optimum mechanism is obtained in *Step* 1. If the workspace of a dimensional mechanism is given with respect to the design specification, the factor D can be achieved from Eq. (20) easily. For example, if the objective workspace is identical with the GCW shown in Fig. 25 in shape and the workspace area is 150 mm^2, the factor D can be obtained as $D = \sqrt{150/3.4817} \approx 6.6$ mm.

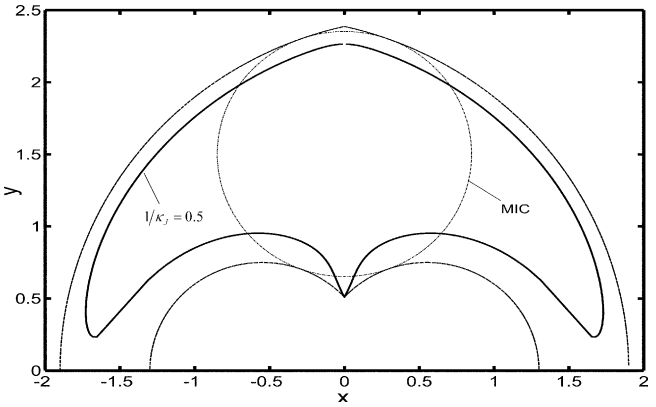

Fig. 25. The GCW restricted by a specified LCI ($1/\kappa_J = 0.5$) for the optimum mechanism with $r_1 = 0.85$, $r_2 = 1.6$ and $r_3 = 0.55$.

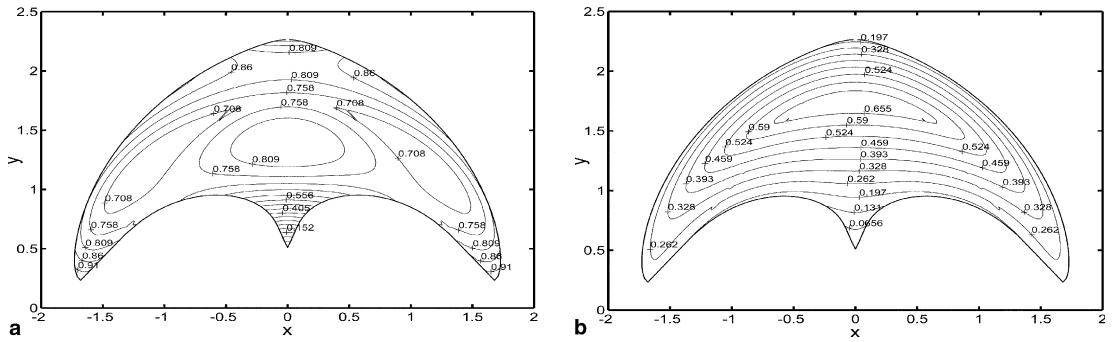

Fig. 26. Distribution of $\|\boldsymbol{D}_{\max}\|$ and $\|\boldsymbol{D}_{\min}\|$ on the GCW for the optimum mechanism with $r_1 = 0.85$, $r_2 = 1.6$ and $r_3 = 0.55$: (a) $\|\boldsymbol{D}_{\max}\|$; (b) $\|\boldsymbol{D}_{\min}\|$.

Step 3: To achieve the dimensional parameters of the optimum mechanism using the dimensional factor D. The relationship between a dimensional parameter and a non-dimensional one is $R_i = Dr_i$. If D is determined, R_i can be achieved. For the above example, there are $R_1 = 5.61$ mm, $R_2 = 10.56$ mm and $R_3 = 3.63$ mm. In this step, one can also check the performances of the dimensional mechanism. For example, Fig. 27 shows the distribution of the LCI and stiffness index on the workspace. From which one can see that the distribution is similar to that when the mechanism is non-dimensional. For the conditioning index, there is no any change. The GCI is still equal to 0.6686. For the stiffness index, it is different in the index value, i.e., $\eta_{D\max} = 33.3475$ and $\eta_{D\min} = 15.7069$. Then, the factor D changes the value of stiffness index but not the conditioning index and the distribution of all indices.

Step 4: To calculate the input limit for θ_1 and θ_2, which can be calculated from the inverse kinematic equation. For the example, the limits are $\theta_1 \in [36.40°, 274.97°]$ and $\theta_2 \in [-94.97°, 143.60°]$, respectively.

Notably, in *Step* 2, the desired workspace can be any shape. It should be determined by the design specification. Whatever the workspace shape is, one can always find a similar downsized workspace. The downsized workspace, which is symmetric about the y-axis, should be maximal included in the obtained GCW. For example, if the desired workspace is a square with the area of 10 mm × 10 mm = 100 mm^2, we can find a maximal square with the area of $1.11 \times 1.11 = 1.2321$ (see Fig. 28) in the GCW. The factor D should be 9.1 mm. The dimensional parameters of the

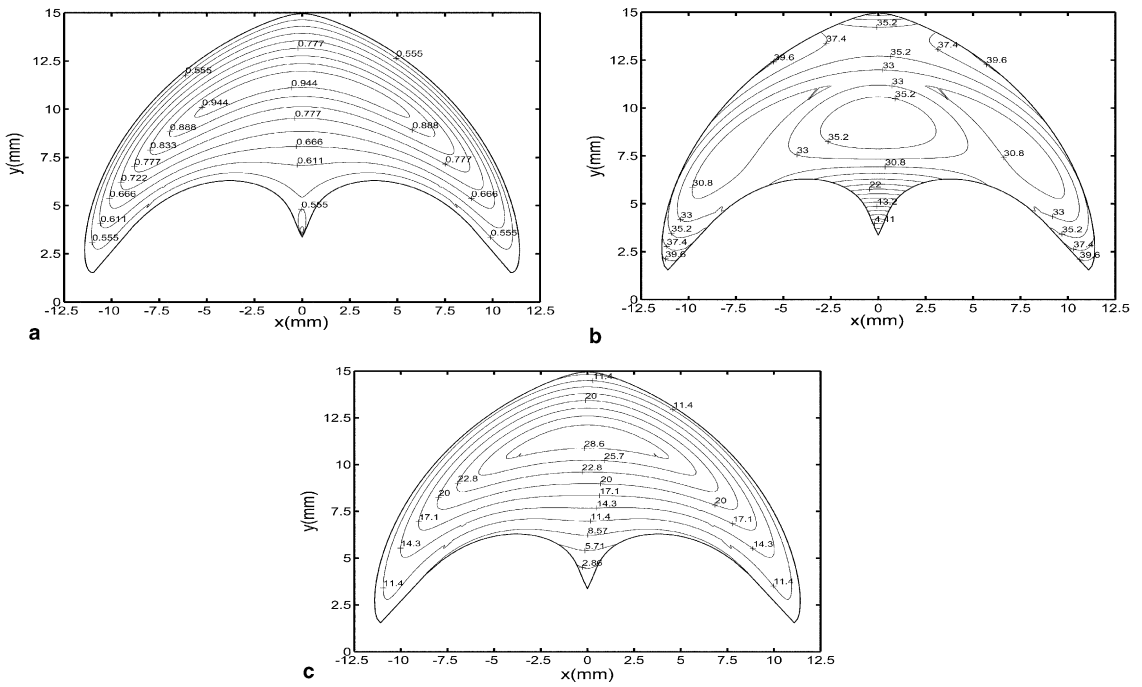

Fig. 27. Distribution of performance indices on the desired workspace for the dimensional optimum mechanism: (a) $1/\kappa_J$; (b) $\|\boldsymbol{D}_{\max}\|$; (c) $\|\boldsymbol{D}_{\min}\|$.

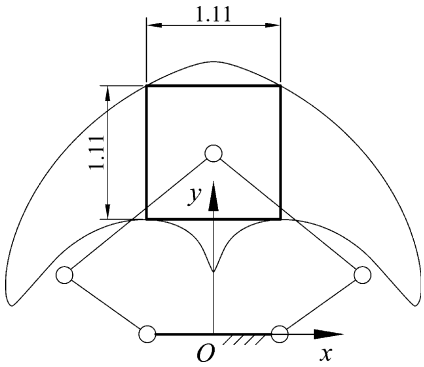

Fig. 28. The maximal included square in the GCW.

design will be $R_1 = 7.74$ mm, $R_1 = 14.56$ mm and $R_1 = 5.0$ mm. The input limits are $\theta_1 \in [84.65°, 216.0°]$ and $\theta_2 \in [-36.0°, 95.35°]$, respectively.

From this section, one can see that all mechanisms with parameters $R_i = Dr_i$ have similar performances to that with the non-dimensional parameters r_i. For example, the workspace of the mechanism with R_i is D^2-time that of the mechanism with r_i. Within the similar workspaces, the GCI values are the same as that of the other. And other performance indices are the same in the distribution on the workspaces and only different in quantity. The mechanisms, which have such a performance similarity, are referred to as the *similarity mechanisms*. Then, the ratios of geometric parameters R_i of all *similarity mechanisms* are constant. Any one of the non-dimensional mechanisms in the established design space stands for all of its possible *similarity mechanisms*. After normalization, a mechanism with any kind of link lengths can find its position in the design space. For such a reason, the design space is a useful tool to present a global comparative result in terms of performances for all mechanisms. This also guarantees a global optimum result in the design issue.

4. Conclusions

In this paper, some indices are defined with respect to the *maximal inscribed workspace* (MIW). As shown in the paper, these indices can be used to evaluate the studied performances, such as control accuracy, dexterity, velocity, payload capability and stiffness. The corresponding atlases are obtained in the established design space, in which any one of the non-dimensional mechanisms stands for all of its possible *similarity mechanisms*. One important advantage of such an atlas is that it can give designers a global and visual information on with what kind of link lengths the mechanism can have good or best performance. As shown by the examples, the atlases can be used in the optimum design process to identify an optimum region, which contains useful information on the geometric parameters. Based on the information, one can select a non-dimensional mechanism directly, or search a most optimal result in further using one classical searching algorithm. Notably, the optimum regions and optimum mechanism examples given in the paper are presented only showing how the optimum design tool and method work. They can be different if

the design specification is changed with respect to a specified application. Anyway, a desired optimum result can be finally achieved using the presented atlases. The optimum regions and mechanism examples with non-dimensional parameters are comparative results. They cannot be used in some applications due to the small workspace. But they stand for all of their own *similarity mechanisms*. Therefore, they are very important to determine a dimensional mechanism for an expected workspace. Comparing the *good-conditioning workspace* of a non-dimensional mechanism with the expected workspace, the dimensional factor D can be obtained. The factor is so important to achieve the final design result as shown in the text. Compared with the traditional optimum design method, the proposed methodology has some advantages as follows: (a) the relationship between an index and design parameters can be illustrated fully in a finite space; (b) the optimum design process can consider multi-criteria, and also guarantees the optimal result; (c) the methodology provides not just one optimum result but an optimum region (contains all possible optimum results); (d) as the optimum design can be carried out by using atlases, this methodology shall be said to be acceptable in practice.

Acknowledgement

The first author wishes to acknowledge the support from the Alexander von Humboldt (AvH) Foundation when he was the AvH Research Fellow at University of Stuttgart in Germany.

This work was supported partly by the National Natural Science Foundation of China (No. 50505023).

References

[1] G. Strang, Linear Algebra and its Application, Academic Press, New York, 1976.
[2] J.K. Salisbury, J.J. Craig, Articulated hands: force control and kinematic issues, The International Journal of Robotics Research 1 (1) (1982) 4–12.
[3] C.A. Klein, B.E. Blaho, Dexterity measures for the design and control of kinematically redundant manipulators, The International Journal of Robotics Research 6 (2) (1987) 72–82.
[4] J. Angeles, C. López-Cajún, The dexterity index of serial-type robotic manipulators, in: Proceedings of the ASME 20th Biennial Mechanisms Conference, Kissimmee, 1988, pp.79–84.
[5] C. Gosselin, J. Angeles, The optimum kinematic design of a planar three-degree-of-freedom parallel manipulators, ASME Journal of Mechanisms, Transmissions, Automations, Design 110 (1) (1988) 35–41.
[6] C. Gosselin, J. Angeles, The optimum kinematic design of a spherical three Degree-of-Freedom parallel manipulator, Journal of Mechanisms, Transmissions, Automations, Design 111 (2) (1989) 202–207.
[7] J. Ryu, J. Cha, Optimal architecture design of parallel manipulators for best accuracy, in: Proceedings of the 2001 IEEE/RSJ International Conference on Intelligent Robots and Systems, Maui, HI, USA, 2001, pp. 1281–1286.
[8] H.S. Kim, L.-W. Tsai, Design optimization of a cartesian parallel manipulator, Journal of Mechanical Design 125 (1) (2003) 43–51.
[9] C. Gosselin, J. Angeles, A global performance index for the kinematic optimization of robotic manipulators, Transaction of the ASME, Journal of Mechanical Design 113 (1991) 220–226.
[10] F. Gao, X. Zhang, Y. Zhao, H. Wang, A physical model of the solution space and the atlases of the reachable workspaces for 2-DOF parallel plane wrists, Mechanism and Machine Theory 31 (2) (1996) 173–184.
[11] F. Gao, X.-J. Liu, W.A. Gruver, Performance evaluation of two-degree-of-freedom planar parallel robots, Mechanism and Machine Theory 33 (6) (1998) 661–668.

[12] X.-J. Liu, The relationships between the performance criteria and link lengths of the parallel manipulators and their design theory, Ph.D thesis, Yanshan University, Qinhuangdao, China, 1999.
[13] J.J. Cervantes-Sánchez, J.C. Hernández-Rodríguez, J. Angeles, On the kinematic design of the 5R planar, symmetric manipulator, Mechanism and Machine Theory 36 (2001) 1301–1313.
[14] D.C. Tao, A.S. Tall, Analysis of a symmetrical five-bar linkage, Product Engineering 23 (1952) 175–177.
[15] T.W. Lee, F. Freudenstein, Synthesis of geared 5-bar mechanisms for unlimited crank rotations and optimum transmission, Mechanism and Machine Theory 13 (1978) 235–244.
[16] H. Zhou, E.H.M. Cheung, Analysis and optimal synthesis of hybrid five-bar linkages, Mechatronics 11 (2001) 282–300.
[17] T. Huang, M. Li, Z. Li, D.G. Chetwynd, D.J. Whitehouse, Optimal kinematic design of 2-DOF parallel manipulators with well-shaped workspace bounded by a specified conditioning index, IEEE Transactions on Robotics and Automation 20 (3) (2004) 538–543.
[18] G. Alıcı, B. Shirinzadeh, Optimum synthesis of planar parallel manipulators based on kinematic isotropy and force balancing, Robotica 22 (2004) 97–108.
[19] X.-J. Liu, J. Wang, G. Pritschow, Kinematics, singularity and workspace of planar 5R symmetrical parallel mechanisms, Mechanism and Machine Theory, in press, doi:10.1016/j.mechmachtheory.2005.05.004.
[20] K.J. Waldron, K.H. Hunt, Series-parallel dualities in actively coordinated mechanisms, Robotics Research 4 (1988) 175–181.